IOP Publishing Journal of Physics D: Applied Physics
J. Phys. D: Appl. Phys. **50** (2017) 085002 (5pp) doi:10.1088/1361-6463/aa5627

Nanocontact based spin torque oscillators with two free layers

R Soucaille[1], J-V Kim[1], T Devolder[1], S Petit-Watelot[2], M Manfrini[3], W Van Roy[3] and L Lagae[3,4]

[1] Centre de Nanosciences et de Nanotechnologies, CNRS, Univ. Paris-Sud, Université Paris-Saclay, 91405 Orsay, France
[2] Institut Jean Lamour, CNRS Université Lorraine, Vandoeuvre-lès-Nancy, France
[3] IMEC, Kapeldreef 75, B-3001 Leuven, Belgium
[4] Lab. Vaste-Stoffysica en Magnetisme, Katholieke Universiteit Leuven, Belgium

E-mail: soucaille@crans.org and thibaut.devolder@u-psud.fr

Received 2 November 2016, revised 16 December 2016
Accepted for publication 30 December 2016
Published 25 January 2017

Abstract

We study a spin torque oscillator based on magnetic vortices hosted by a pseudo spin valve, and generated and confined by a nanocontact configuration. In addition to the standard functioning modes of such spin torque oscillators, we present evidence for field and current conditions leading to a novel extinction regime, where the oscillator response is transiently quenched. We model the dynamics analytically for two non-interacting vortices, one in each magnetic layer. The similarity of their trajectories makes them prone to interact. We argue that they can synchronize and then follow identical orbits, which leads to the extinction of the RF voltage emission.

Keywords: magnetic vortex, oscillator, spin transfer torque

(Some figures may appear in colour only in the online journal)

1. Introduction

Spin torque oscillators are designed with a rich variety of configurations that allow the manipulation of various magnetization textures [1] and the exploration of such novel phenomena as synchronization [2] and chaos [3]. They promise to be some of the key building blocks of the future spintronics [4]. Nanocontacts (NCs) on magnetic multilayers are a system of choice for the implementation of spin torque oscillators: indeed, depending on the manipulated magnetic texture they offer frequency tunabilities [5] from tens of GHz for spin-wave bullets [6] or droplet-based oscillators [7] to deeply sub-GHz bands for the vortex-based oscillators [8] that we shall focus on here.

In NCs there is no shape anisotropy. As a result one relies on the Oersted–Ampere field created by the current to favour the nucleation of a vortex in the free layer. The vortex is set into orbital motion about the NC by the spin transfer torque arising from the in-plane current (CIP) [9]. In most cases, the magnetic stack is a spin-valve, i.e. composed by a dynamically active free layer and an essentially static reference layer, which only acts as a spin polarizer for the current. While the dynamics is well understood in the case of a heavily pinned—hence static polarizing—layer, little is known about the pseudo spin-valve (pSV) case when the polarizing layer is left free to undergo some dynamics. An intriguing question is whether both magnetic layers can host a moving vortex.

In this paper we tackle that question, by studying the case of a spin torque oscillator based on an NC deposited on a pSV. We will see that such a pSV allows new dynamical states where the microwave emission is quenched in appropriate applied current and fields, which is interpreted as a synchonization of vortices. This leads to a continuously rotating rigid mutual configuration for the two magnetization textures in a certain range of current.

2. Experimental methods

Our samples are based on pSVs of composition Pt(4 nm, cap)/ Co(5)/ Au(5)/ Co(10)/ Au(30)/ Pt(5)/ substrate. Hysteresis loops (not shown) indicate that the thickest Co layer is the hardest; it exhibits a coercivity of 10–15 mT, depending on the

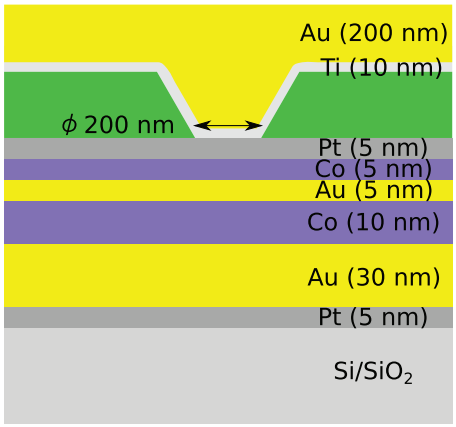

Figure 1. Sketch of the nanocontact geometry. The magnetic stack is based on a pSV where the dynamic of the two cobalt layers can be excited.

device. In field-induced switching, the thinnest Co layer plays the role of a free layer, since it has a typically five times lower coercivity. The NC is an inverted cone made of Au(200 nm) on Ti(10 nm). Its diameter is 200 nm at its contact with the pSV. Overall, this leads to a resistance of 9 Ω with a magnetoresistance of 21 mΩ. A sketch of the NC is shown in figure 1.

To nucleate the vortices and trigger their dynamics, we apply a dc current ($0 \leqslant I_{DC} \leqslant 60$ mA) through the NC. This current is modulated and a lock-in technique yields the differential resistance of the NC. Due to Joule heating the NC resistance has a quadratic increase with respect to the current; to exhibit small but abrupt change in the resistance this contribution is removed in figure 3.

The vortex dynamics is known [8, 10] to make the NC resistance oscillate. Experimentally, these oscillations are analyzed by looking at the spectral density of the NC voltage noise. To this end, we use a bias tee to separate the modulated dc voltage drop in the NC from its high frequency components (10 MHz–2 GHz), that are sent to a spectrum analyzer after amplification.

To prepare vortices and set them in motion, we mostly use the following method: we first saturate the sample by applying a field of 16 mT along the in-plane direction. At this field, the current is then increased from $I_{DC} = 0$ mA to 60 mA. The in-plane field is then decreased quasi-statically to −3 mT. This protocol has proved to lead systematically to self-sustained vortex gyration in the system. We then set the targeted applied fields. Finally we study the dynamics by sweeping the current back to zero, while recording both the NC differential resistance and the voltage noise spectrum it delivers to the amplifiers.

3. Results and modelling

3.1. Experimental results

In zero in-plane field, our pSV-based system exhibits behaviour similar to previous reports on spin-valve based systems [1, 5, 10], consistent with a gyrational motion of vortices. Indeed, upward current sweeps in the NC induce vortex nucleation, which is seen as a reproducible jump of 2.8 mΩ in the

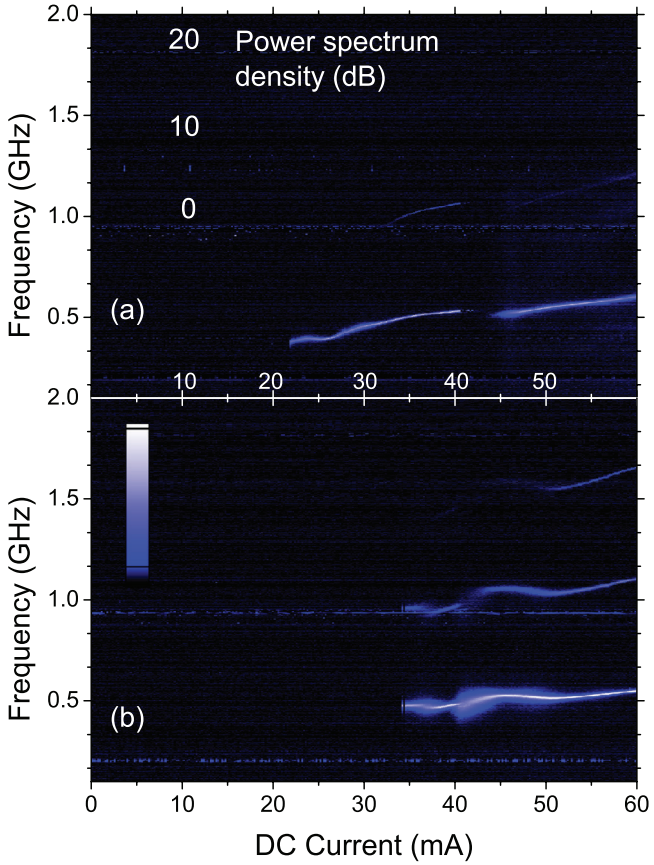

Figure 2. Map of the emitted power spectrum in dB above the noise level by a NC. A 1.2 mT in-plane field is applied in both panels. Panel (a) is the *extinction* case and (b) corresponds to the *normal* case and panel. Panel (b) shows more harmonics due to the higher emitted power at high current.

resistance, concomitant with the appearance of a series of harmonically related peaks in the voltage spectra. The fundamental frequency is linear with the current, with a slope of 5.2 MHz · mA^{-1}.

This apparent similarity of the behavior of our pSV with spin valve systems ends as soon as an in-plane field is applied. Let us for instance describe the influence of an in-plane field of 1.2 mT. In this case, the sample dynamics is no longer reproducible. The sample behaviour can be separated into two categories, which we shall refer to as (i) the *extinction* case, and (ii) the *normal* case, sketched in figures 2(a) and (b). Both dynamics occur for the same current and in-plane field.

(i) The first kind of response (figure 2(a)) involves a transient sudden reversible extinction of the RF emission at $I_{DC} = 41$ mA followed by the appearance of a new dynamics at 46 mA. The microwave quiet state has a differential resistance suddenly incremented by typically 5 mΩ (figure 3). When in the extinction case, the critical current for which the RF emission disappears irreversibly is 21 mA. At high currents ($I_{DC} > 50$ mA) the frequency stays linear with the current, with a slope of 5.6 MHz mA^{-1}.

Notably, the current range in which extinction occurs can be tuned by applying a small out of plane field. For

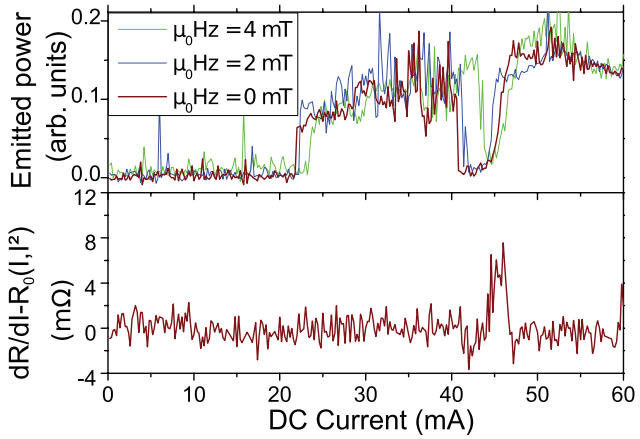

Figure 3. Total emitted voltage power (top panel) and differential resistance (bottom panel) versus the applied current for 1.2 mT in-plane field along the easy axis in the case of the *extinction* response. To show the small change in differential resistance, the differential resistance is fitted by a quadratic function and only the difference between the differential resistance and the fitting function is shown.

instance, the extinction interval ranges from $\Delta I_{ext} = 5$ mA at $\mu_0 H_\perp = 0$ mT to $\Delta I_{ext} = 2.6$ mA at $\mu_0 H_\perp = 4$ mT.

(ii) Conversely, in the second category (figure 2(b)), there is neither an RF extinction nor a perceptible change of the NC differential resistance during a downward sweep of the current. More strikingly, the emitted power is about ten times higher at high current that it was in case (i), and the critical current is higher at 34 mA. The tunability is 4.6 MHz mA^{-1}, i.e. substantially smaller than in case (i), which leads to a decrease of 52 MHz of the voltage peak frequency at 60 mA.

3.2. Modelling with the rigid vortex approximation

To shed light on the extinction phenomenon that appears in pSV but not in SV systems, we have considered the presence of free vortices in both the free and reference magnetic layers. Let us then consider the dynamics in the case of two rigid vortices, one in each layer. For a start, we consider these two vortices as non-interacting and we do not consider the effect of applied magnetic field. The modelling proceeds in three steps.

(i) First, the Oersted field profile and the current distribution are computed numerically, following [9]. The current comprises in-plane components (CIP current) that radiate outwards from the NC and decay in a manner essentially inversely proportional to the distance from the NC center. Far away from the NC, the current densities in both layers are equal. Close to the NC, the current density is larger in the 5 nm thick cobalt layer. The current also comprises components perpendicular to the sample plane (CPP current) with a profile roughly constant underneath the NC, and vanishing everywhere else. The Oersted field profile close to the NC resembles that generated by a semi-infinite cylindrical distribution of current: the field is roughly linear below the NC, and is inversely proportional to the distance away from the NC.

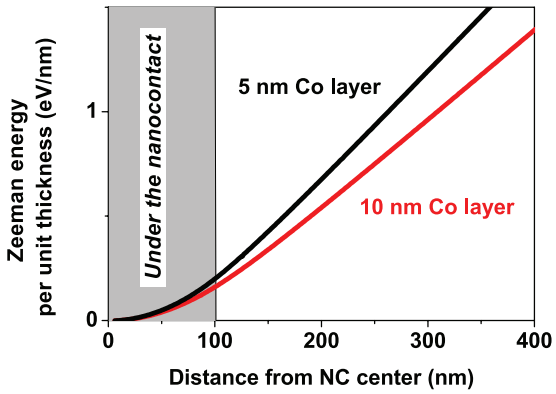

Figure 4. Calculated Zeeman confinement for rigid vortices in each magnetic layer. The Zeeman confinement energy per unit thickness is shown for clarity.

(ii) We then apply the rigid vortex approximation where the only dynamics involves the translation of the two vortex cores. From the Oersted field profile, some algebra leads to the vortex Zeeman energies in each layer (see appendix). As expected, the Zeeman potentials (figure 4) are similar for both cobalt layers and depend only on the distance between the NC and the vortex core. More specifically, the vortices feel potentials which result in forces that attract them towards a point below the center of the NC. The confinement is slightly stronger in the top cobalt layer, because the Oersted field is slightly larger (by about 20%). In addition, it is worth noting that the Zeeman potential (figure 4) is more conical than parabolic: its gradient—the Zeeman force acting on the vortex—will be essentially independent of the vortex position when outside the NC area.

(iii) The last modelling step is to account for the dynamics of the vortices by using the Thiele's equation [11],

$$\mathbf{G} \times \frac{\mathrm{d}\mathbf{X}}{\mathrm{d}t} + D\alpha \frac{\mathrm{d}\mathbf{X}}{\mathrm{d}t} + \mathbf{F}_{\mathrm{STT}} + \mathbf{F}_{\mathrm{int}} + \frac{\partial U}{\partial \mathbf{X}} = 0 \qquad (1)$$

where X is the vortex position, U its energy, αD are damping constants, and $\mathbf{G}$ its gyrovector. $\mathbf{F}_{\mathrm{STT\,CIP}}$, $\mathbf{F}_{\mathrm{STT\,CPP}}$, $\mathbf{F}_{\mathrm{int}}$ are the forces resulting from the spin transfer torque (STT) for CIP currents, CPP currents and from the external forces comprising vortex–vortex dipolar interactions.

For the NC geometry it has been shown [3] that the most relevant force inducing the dynamics is the adiabatic STT coming from the CIP current. This force can be written as

$$\mathbf{F}_{\mathrm{STT\,CIP}} = -\mathbf{G} \times \mathbf{u}(\mathbf{X}) \qquad (2)$$

where $\mathbf{u}(\mathbf{X})$ is the spin drift velocity [12]. For a circular motion of the vortex at constant velocity, equation (1) can be reduced to

$$|\mathbf{G}|^2 \cdot u(R) = D\alpha \frac{\partial U}{\partial R} \qquad (3)$$

where R is the radius of the orbit of the vortex. Let us stress that for NCs, there is no confinement due to the geometry, such that both the driving forces (the Zeeman potential) and

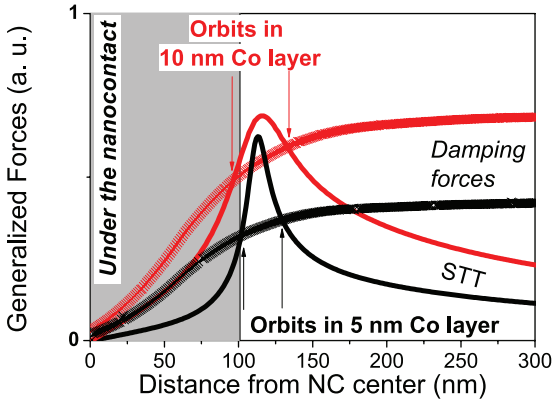

Figure 5. Calculated generalized forces acting on the vortices. The force compensation points are the possible steady state vortex orbits.

the STT are proportional to the current. This leads to the conclusion that the vortex orbits about the NC at a radial distance which is *independent* from the current when no in-plane field is applied—this will be discussed further in point (b) of the next section. The only condition is the existence of the vortex. In our case, equation (2) leads to an orbit radius of 129 nm for a vortex in the thinnest Co layer and 132 nm for a vortex in the thickest Co layer. (The first graphical solution in figure 5 is unstable.) These two orbits are very close to each other (see figure 5) because the cobalt layers have similar properties and are subject to comparable Oersted fields and current profiles.

4. Discussion and concluding remarks

A possible consequence of the proximity of the vortex orbits is that the vortices of each layer may be prone to interact strongly. Experimentally, the frequency is always in the same range of magnitude for all realizations of experiment. Vortices can interact by at least two means.

(a) The first straightforward interaction is the dipolar interaction between the vortex cores [13]. Micromagnetic simulations of the vortex core using the OOMMF package [14] give core radii of 14 and 16 nm for the thinnest and thickest cobalt layers. Although the dipolar core-to-core interaction has a small range, it extends to a few times the vortex core sizes, such that the previously calculated radii of the orbits lead inevitably to dipolar interactions between the cores. The sign of the interaction depends on the relative core polarities: it is repulsive for antiparallel magnetized cores—that always rotate in opposite senses, but it is attractive for parallel polarized cores—that rotate in the same sense. We conjecture that this last situation may lead to a strongly-coupled two-vortex state, that rotates about the nanocontact in such a manner that the relative angle between the two magnetizations is constant in time everywhere. In that case, an extinction of the vortex signal is expected.

(b) The second vortex–vortex interaction is related to the CPP component of the STT. By itself, this torque does not generate self-sustained gyration of the vortex if the in-plane magnetization of the polarizer is uniform. However, if the polarizer were to host a vortex below the NC, it would be magnetized non uniformly. In such a hypothetical case, the CPP torque would lead to a dynamical interaction [15, 16] between the two magnetic layers, and the possible onset of a locked state and the resultant RF extinction.

Experimentally, we can shift the vortex orbit so that it passes below the NC by applying in-plane fields that tilt the confinement profile. Applying in-plane fields is thus a way to promote this interaction through CPP STT and to facilitate the interaction between the two vortices [17]. In this case the orbit is no longer circular and the distance will depend on the current making vortices interact for certain current range. This is qualitatively consistent with the experimental fact that extinction happens only when an in-plane field is applied. The CPP torque is also tuned by the perpendicular magnetic field [10]. $H_\perp$ induces an extra out-of-plane component of the magnetization, independent of the vortex core position. This out-of-plane spin polarization of the CPP current can split the vortex dynamics, making two vortices less prone to synchronize—as seen in figure 3. The validation of this scenario is, however, beyond the scope of the present study.

In summary, we have studied a cobalt-based pVS system in a nanocontact configuration. At zero applied field, the system appears to function like standard vortex-based spin torque oscillators, with properties in line with previous findings. However when applying in-plane fields, there exist current conditions leading to a novel extinction regime, where the oscillator response is transiently suppressed before it can be reactivated at different applied currents. We have modelled the system dynamics analytically by considering two rigid non-interacting vortices, one in each cobalt layer. The similarity of the trajectories of the two vortices make them prone to interact. We interpret the extinction as their synchronization along essentially identical orbits. Exacerbating one of the vortex–vortex interaction mechanisms by using an in-plane field facilitates the extinction, which is consistent with our interpretation.

Appendix. Zeeman potential

The Zeeman potential is expressed as

$$U_{\text{zeeman}} = -\frac{1}{2}\mu_0 \int\int\int \mathbf{M}\cdot\mathbf{H}\,\mathrm{d}V. \tag{A.1}$$

For a vortex both Oersted field (**H**) and magnetization (**M**) have a cylindrical symmetry. We assume the magnetization to be uniform across the thickness for both free and reference layers, since the layer thicknesses are small compared with the exchange length in cobalt. By assuming that the vortex is at a radial distance R_0 from the nanocontact, we can write these quantities in polar coordinates in the following way,

$$\mathbf{H}(r,\theta) = H(r)\mathbf{e}_\theta, \tag{A.2}$$

$$\mathbf{M}(r,\theta)\cdot\mathbf{e}_\theta = \frac{r - R_0\sin(\theta)}{\sqrt{R_0^2 + r^2 - 2R_0 r\sin(\theta)}}. \tag{A.3}$$

$$U_{\text{Zeeman}} = -\frac{\mu_0 d}{2}\int_{r=0}^{+\infty} H(r)\ M_s \times\left[(r-R_0)K\left(\frac{4R_0 r}{(r+R_0)^2}\right)+(r+R_0)E\left(\frac{4R_0 r}{(r+R_0)^2}\right)\right]\mathrm{d}r. \tag{A.4}$$

Integrating the θ parameter between 0 and 2π leads to equation (A.4), where K and E are respectively the complete elliptic integral of the first kind and the complete elliptic integral, M_s is the magnetization in $\mathrm{A}\cdot\mathrm{m}^{-1}$, H the Oersted field in $\mathrm{A}\cdot\mathrm{m}^{-1}$, and d the thickness.

References

[1] Manfrini M, Kim J-V, Petit-Watelot S, Van Roy W, Lagae L, Chappert C and Devolder T 2014 Propagation of magnetic vortices using nanocontacts as tunable attractors *Nat. Nanotechnol.* **9** 121–5

[2] Kaka S, Pufall M R, Rippard W H, Silva T J, Russek S E and Katine J A 2005 Mutual phase-locking of microwave spin torque nano-oscillators *Nature* **437** 389–92

[3] Petit-Watelot S, Kim J-V, Ruotolo A, Otxoa R M, Bouzehouane K, Grollier J, Vansteenkiste A, Van de Wiele B, Cros V and Devolder T 2012 Commensurability, chaos in magnetic vortex oscillations *Nat. Phys.* **8** 682–7

[4] Locatelli N, Cros V and Grollier J 2014 Spin-torque building blocks *Nat. Mater.* **13** 11–20

[5] Manfrini M, Devolder T, Kim J-V, Crozat P, Zerounian N, Chappert C, Van Roy W, Lagae L, Hrkac G and Schrefl T 2009 Agility of vortex-based nanocontact spin torque oscillators *Appl. Phys. Lett.* **95** 192507

[6] Slavin A and Tiberkevich V 2005 Spin wave mode excited by spin-polarized current in a magnetic nanocontact is a standing self-localized wave bullet *Phys. Rev. Lett.* **95** 237201

[7] Mohseni S M *et al* 2013 Spin torque generated magnetic droplet solitons *Science* **339** 1295–8

[8] Pufall M R, Rippard W H, Schneider M L and Russek S E 2007 Low-field current-hysteretic oscillations in spin-transfer nanocontacts *Phys. Rev.* B **75** 140404

[9] Petit-Watelot S, Otxoa R M and Manfrini M 2012 Electrical properties of magnetic nanocontact devices computed using finite-element simulations *Appl. Phys. Lett.* **100** 083507

[10] Mistral Q, van Kampen M, Hrkac G, Kim J-V, Devolder T, Crozat P, Chappert C, Lagae L and Schrefl T 2008 Current-driven vortex oscillations in metallic nanocontacts *Phys. Rev. Lett.* **100** 257201

[11] Kim J-V 2012 Spin-torque oscillators *Solid State Physics* vol 63 ed R E Camley and R L Stamps (Academic) pp 217–94

[12] Thiaville A, Nakatani Y, Miltat J and Suzuki Y 2005 Micromagnetic understanding of current-driven domain wall motion in patterned nanowires *Europhys. Lett.* **69** 990

[13] Cherepov S S, Koop B C, Galkin A Y, Khymyn R S, Ivanov B A, Worledge D C and Korenivski V 2012 Core–core dynamics in spin vortex pairs *Phys. Rev. Lett.* **109** 097204

[14] Donahue M J and Porter D G 1999 OOMMF user's guide, version 1.0 *Interagency Report* NISTIR 6376, National Institute of Standards and Technology, Gaithersburg, MD

[15] Khvalkovskiy A V, Grollier J, Locatelli N, Gorbunov Y V, Zvezdin K A and Cros V 2010 Nonuniformity of a planar polarizer for spin-transfer-induced vortex oscillations at zero field *Appl. Phys. Lett.* **96** 212507

[16] Sluka V, Kákay A, Deac A M, Bürgler D E, Hertel R and Schneider C M 2012 Quenched Slonczewski windmill in spin-torque vortex oscillators *Phys. Rev.* B **86** 214422

[17] Otxoa R M, Petit-Watelot S, Manfrini M, Radu I P, Thean A, Kim J-V and Devolder T 2015 Dynamical influence of vortex–antivortex pairs in magnetic vortex oscillators *J. Magn. Magn. Mater.* **394** 292–8